13A.3 COMPARISON OF MIXING LAYER HEIGHT RETRIEVED BY CEILOMETER AND DOPPLER LIDAR

Joshua Vande Hey *
University of Leicester, Leicester, UK

Judith Agnew
STFC, Didcot, UK

James Richards, Ranvir Dhillon, and Mike Brettle
Campbell Scientific, Ltd., Shepshed, UK

1. INTRODUCTION

Boundary layer mixing height strongly influences air quality since concentrations at the surface decrease with the amount of mixing taking place (Holzworth 1967). A variety of ground-based remote sensing instruments have been used to profile the boundary layer (e.g. Barlow et al. 2011). This paper is concerned primarily with comparing two types of instrument: Doppler lidar and ceilometer, to evaluate the capabilities of an automated, ceilometer-based convective mixing layer height (MLH) retrieval.

Doppler lidar systems have been used to profile boundary layer meteorology by monitoring aerosol backscatter and vertical velocity of aerosols and cloud particles (Pearson et al. 2008, O'Connor et al. 2010, Barlow et al. 2011, Harvey et al. 2013). Laser ceilometers have been used to deduce the MLH through detection of negative gradients in aerosol returns (Munkel and Rasanen 2004, Wiegner et al. 2006, de Haij et al. 2007, Haeffelin et al. 2012). Ceilometer-based MLH retrievals are sometimes challenging, for example during stable night time conditions when it can be difficult to discern mixed from residual layers by backscatter gradients alone (Haeffelin et al. 2012), or when aerosol loading is very low. However, ceilometers are low-cost instruments deployed in large networks around the world and therefore have strong potential to provide continuous monitoring of the boundary layer not feasible with traditional techniques such as radiosonde profiling.

Here, an operational mixing layer height retrieval algorithm based on the gradient method of de Haij et al. (2007) is described and applied to a Campbell Scientific CS135 ceilometer along with a quality factor scheme, and retrievals are compared with mixing layer heights derived using a HALO Photonics Doppler lidar at Chilbolton Observatory in Hampshire, UK. In addition, the Doppler lidar + sonic anemometer boundary layer typing scheme of Harvey et al. (2013) is applied to provide additional information on the state of the boundary layer. The performance of the ceilometer MLH retrieval is assessed under a variety of wintertime atmospheric conditions.

* *Corresponding author address:* Joshua Vande Hey, Univ. of Leicester, Dept. of Physics and Astronomy, Earth Observation Science Group; email: jvh7@le.ac.uk .

2. CEILOMETER MLH ALGORITHM

A description of the prototype instrument design upon which the CS135 was based can be found in VandeHey et al. (2012). The instrument transmits 905nm laser light in 3μJ pulses of 100ns duration at a 10kHz repetition rate. A 30MHz sampling rate provides 5m range detection resolution, while the 100ns laser pulse can be vertically resolved to 15m.

The CS135 mixing layer height detection scheme is based to some extent on the gradient peak method as described by de Haij et al. (2007), though the quality scheme described below is unique to the CS135. Aerosols are used as tracers for convective mixing, and the aerosol backscatter signal is used to identify a transition between the mixed layer and the layer above. In the peak method described by de Haij et al. (2007), layers are assigned at heights where local minima in backscatter gradient and local maxima in backscatter variance are co-located, provided the backscatter gradient meets defined threshold criteria.

The CS135 MLH algorithm is applied as follows. First, the signal is preconditioned and range and overlap correction are applied. Overlap is calculated as in Vande Hey et al. (2011). The data are then smoothed and truncated as described in Table 1.

Table 1. CS135 MLH filtering settings.

Parameter	Default Setting
Time averaging	30 minute running average
Range smoothing	150m Gaussian range-smoothing
Standard Deviation	150m window (Δ = 75m)
Maximum MLH range	3000m or lowest detected cloud base, whichever is smaller

Note that while clouds are often part of boundary layer structures, the gradient in the backscatter signal from a cloud base can be much steeper than that in the signal from the top of an aerosol layer. In order to reduce the probability that cloud backscatter hides the

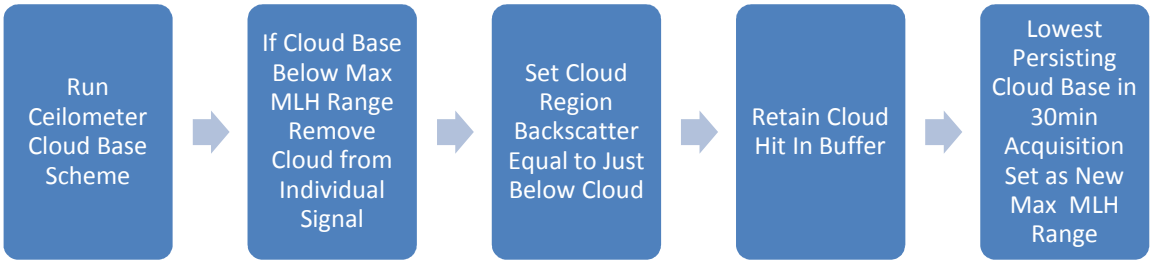

FIG. 1. Process for removing cloud backscatter signals from MLH algorithm input.

aerosol backscatter profile, cloud bases in the boundary layer are currently removed from the input of the MLH algorithm by application of the process shown in Fig. 1.

After clouds are removed, a gradient detection process is applied to identify up to three peak negative gradients. Up to three MLH outputs are given in cases where more than one aerosol layer is present, for example when a mixed layer, a residual layer, and an aerosol layer aloft are all present. The slope of the backscatter signal is calculated at each detection range of the instrument, and minima are identified. The candidate range-dependent gradients are assessed by a quality factor, $Q(\mathrm{r})$, defined as

$$Q(\mathrm{r}) = \left. -\frac{d\beta_s(\mathrm{r})}{d\mathrm{r}} \right/ \sigma_{\beta_0}(\mathrm{r}-\Delta{:}\,\mathrm{r}+\Delta) \qquad (1)$$

where $\beta_s(\mathrm{r})$ is the range-smoothed backscatter, r is the range, and σ_{β_0} is the standard deviation of the non-range-smoothed backscatter in the region within r±Δ. The likelihood of an identified minimum gradient corresponding to an aerosol layer structure is indicated by the following quality factor ranges that were set based on manual analysis of training data sets.

$$\begin{array}{ll} If\ 1.8 \le Q(r) < 5 & layer\ possible \\ If\ 5 \le Q(r) < 10 & layer\ likely \\ If\ Q(r) \ge 10 & layer\ highly\ likely \end{array} \qquad (2)$$

By requiring these specified ratios of gradient to standard deviation of backscatter, spurious peaks resulting from instrument noise are suppressed.

2. METHOD FOR ASSESSING THE ALGORITHM

In order to assess the performance of the CS135 MLH algorithm, the instrument outputs were compared with other measurements at Chilbolton Observatory in Hampshire, UK. The 1550nm HALO Photonics Doppler lidar (STFC, 2014) was used as the primary reference, but the data from the Metek USA-1 sonic anemometer (STFC, 2014b) also used through an algorithm developed by Harvey et al. (2013) which incorporates Doppler lidar and sonic anemometer data to identify boundary layer type. The method of Harvey et al. was applied through use of published code (Harvey 2014).

The algorithm of Harvey et al. automatically classifies the boundary layer type through a probabilistic approach which weights the likelihood of each of the types listed in Table 2. This classification scheme is a modified version of the scheme in Lock et al. (2000). See Harvey et al. (2013) for illustrations of these types.

Table 2. Boundary layer types of Harvey et al. 2013.

Type ID	Description
Ia	Stable boundary layer, no cloud
Ib	Stratus-topped stable boundary layer, no cumulus
Ic	Forced cumulus under stratocumulus
II	Decoupled stratocumulus over stable surface layer
IIIa	Single mixed layer, no cloud
IIIb	Single stratocumulus-topped mixed layer, no cumulus
IV	Decoupled stratocumulus
V	Decoupled stratocumulus over cumulus
VI	Cumulus capped layer

The CS135 MLH scheme and the Harvey PBL classification algorithm were run on 31 days of data gathered at Chilbolton during the winter month of December, 2013. A few of the days have been selected as example cases, and some summary statistics follow.

3. EXAMPLE DATA

Five days of example data are shown in Fig. 2 to Fig. 6 to illustrate how the ceilometer MLH relates to the Doppler data and the Harvey Classification scheme.

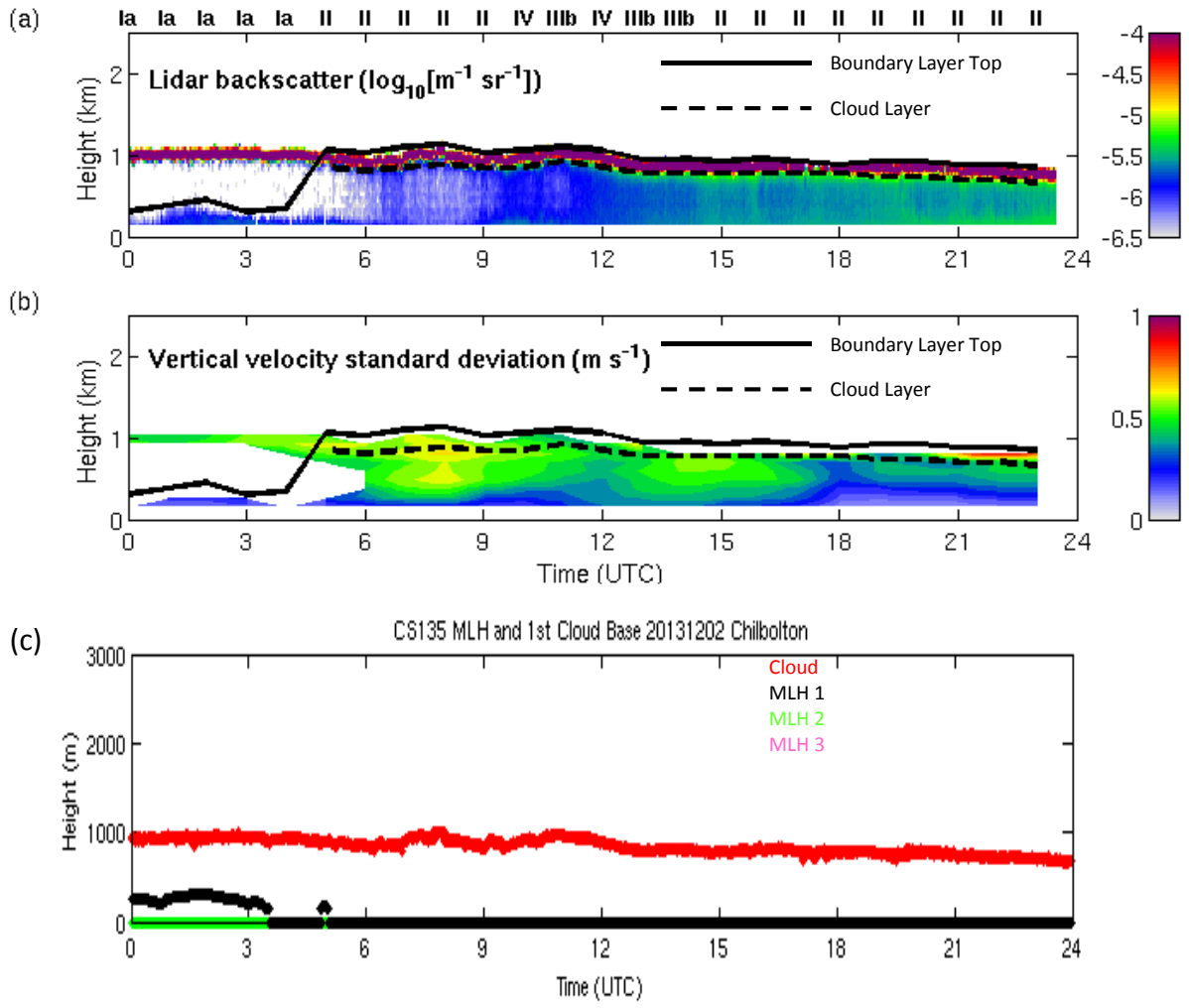

FIG. 2. Halo Doppler lidar data and CS135 ceilometer data from Chilbolton Observatory on 2 December 2013. Panel a) shows the logarithmic lidar backscatter with boundary layer top (height of transition from boundary layer to free troposphere) and cloud layer locations output by the Harvey algorithm, panel b) shows the vertical velocity standard deviation, again with the boundary layer top and cloud layer top output by the Harvey algorithm, and panel c) shows layers reported by the ceilometer. Along the top of panel a) are the boundary layer types retrieved by the scheme of Harvey et al. (2013) as described in Table 2. Panels a) and b) both show cloud layers and top of planetary boundary layer as reported by Harvey's algorithm. Panel c) shows the lowest cloud layer reported by the ceilometer along with up to three mixing layer heights (MLH). In this example, the aerosol content is low throughout the day and a pervasive cloud layer prevents the CS135 ceilometer from retrieving mixing layer after the first three hours of the day.

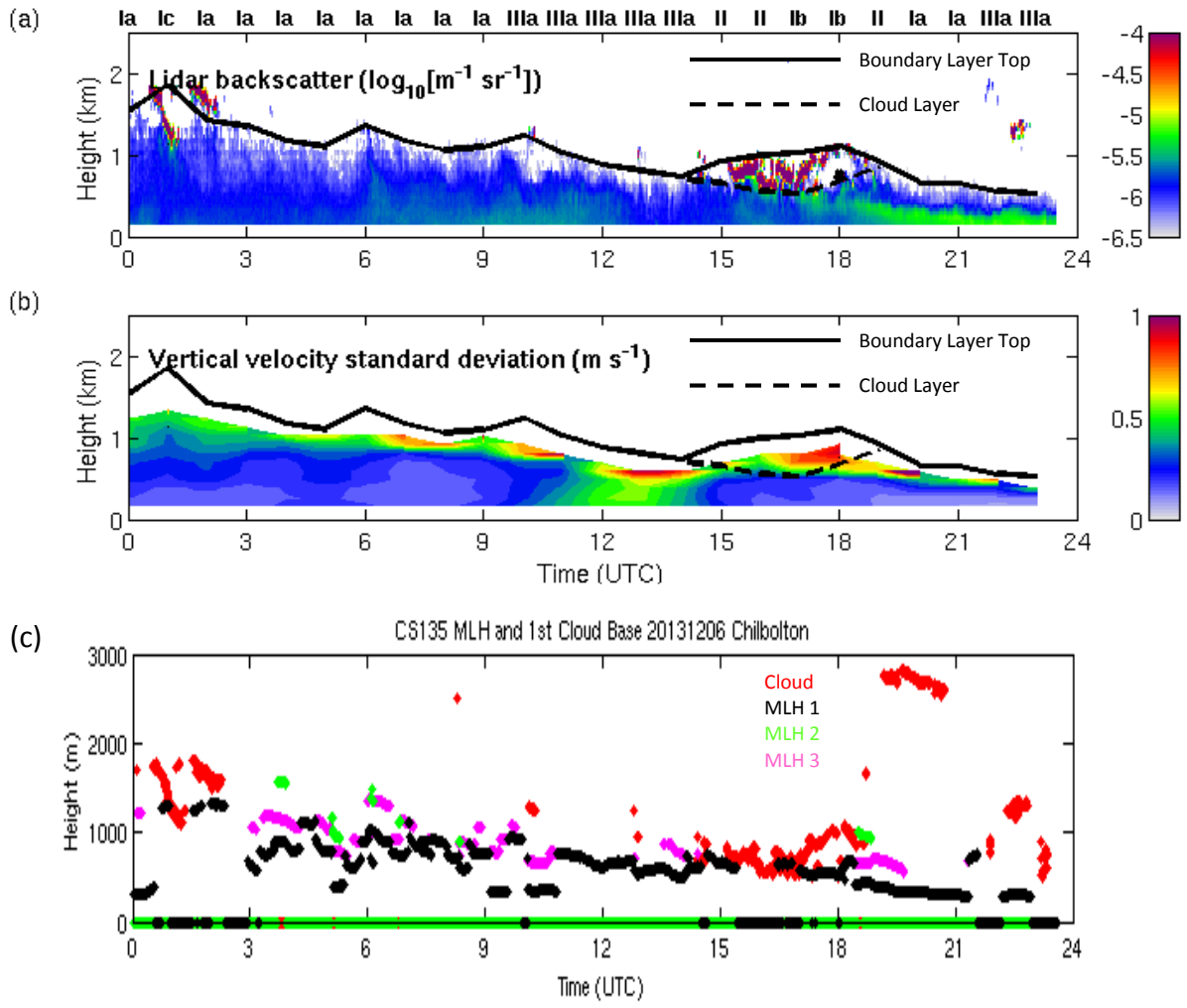

FIG. 3. Same as Fig. 2 except from 6 December 2013. On this mostly cloud free day, the ceilometer reported mixing layer heights throughout most of the day. Around 09:00 the instrument reported two layers which might correspond to a lower mixed layer and a higher residual layer. This occurs after the Harvey algorithm reports a transition from stable to mixed boundary layer, but the lower aerosol layer is visible in the Doppler data before this. The same situation occurs between 18:00 and 19:30, though in this case the boundary layer has been classified predominantly as stable.

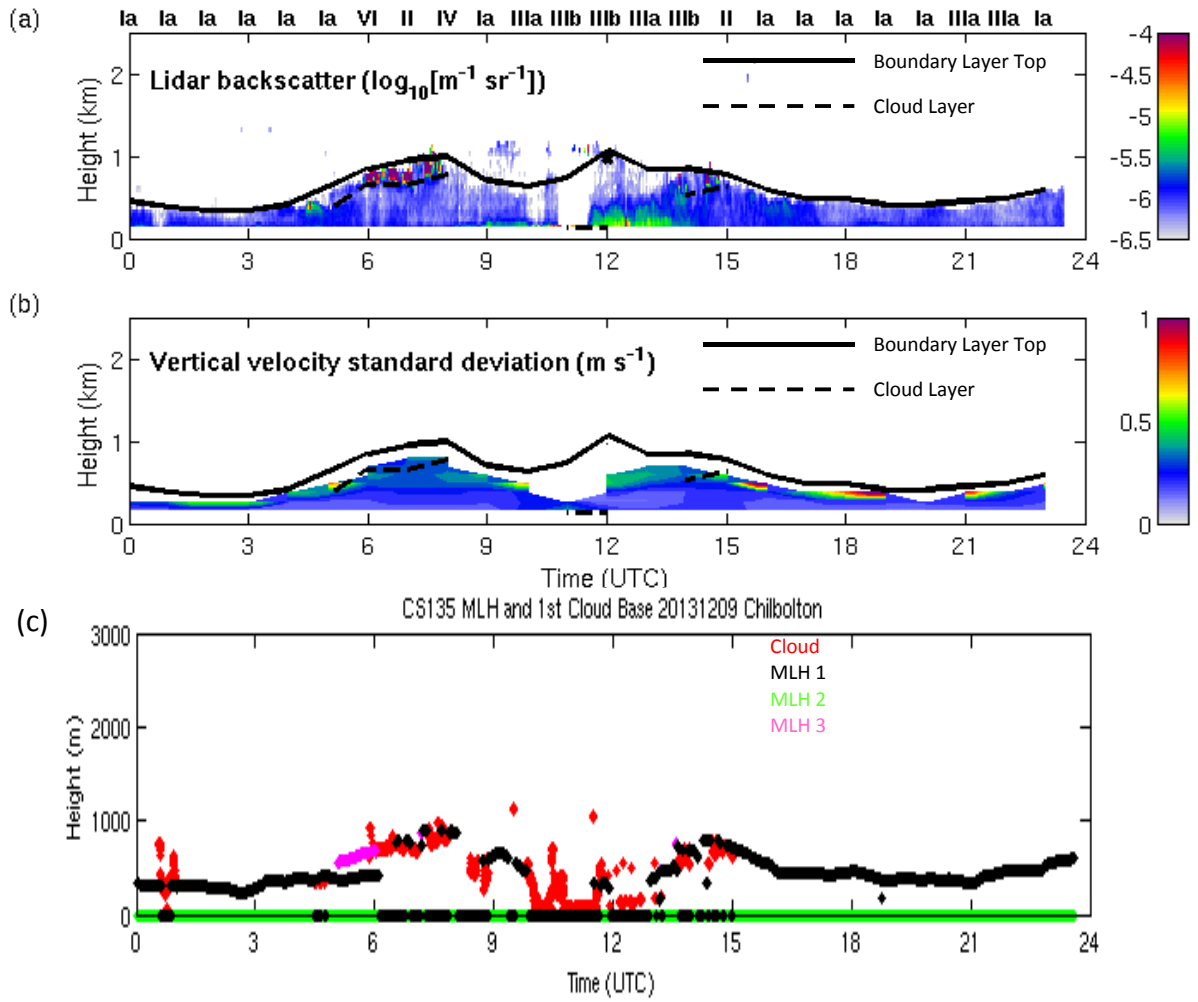

FIG. 4. Same as Fig. 2 except from 9 December 2013. Here the CS135 reports a mixing layer height that tracks the Doppler lidar-derived PBL height, except between 10:00 and 13:00 when a very low cloud layer is reported. Situations where MLH was not reported in the presence of very low cloud occurred in several of the cases analysed.

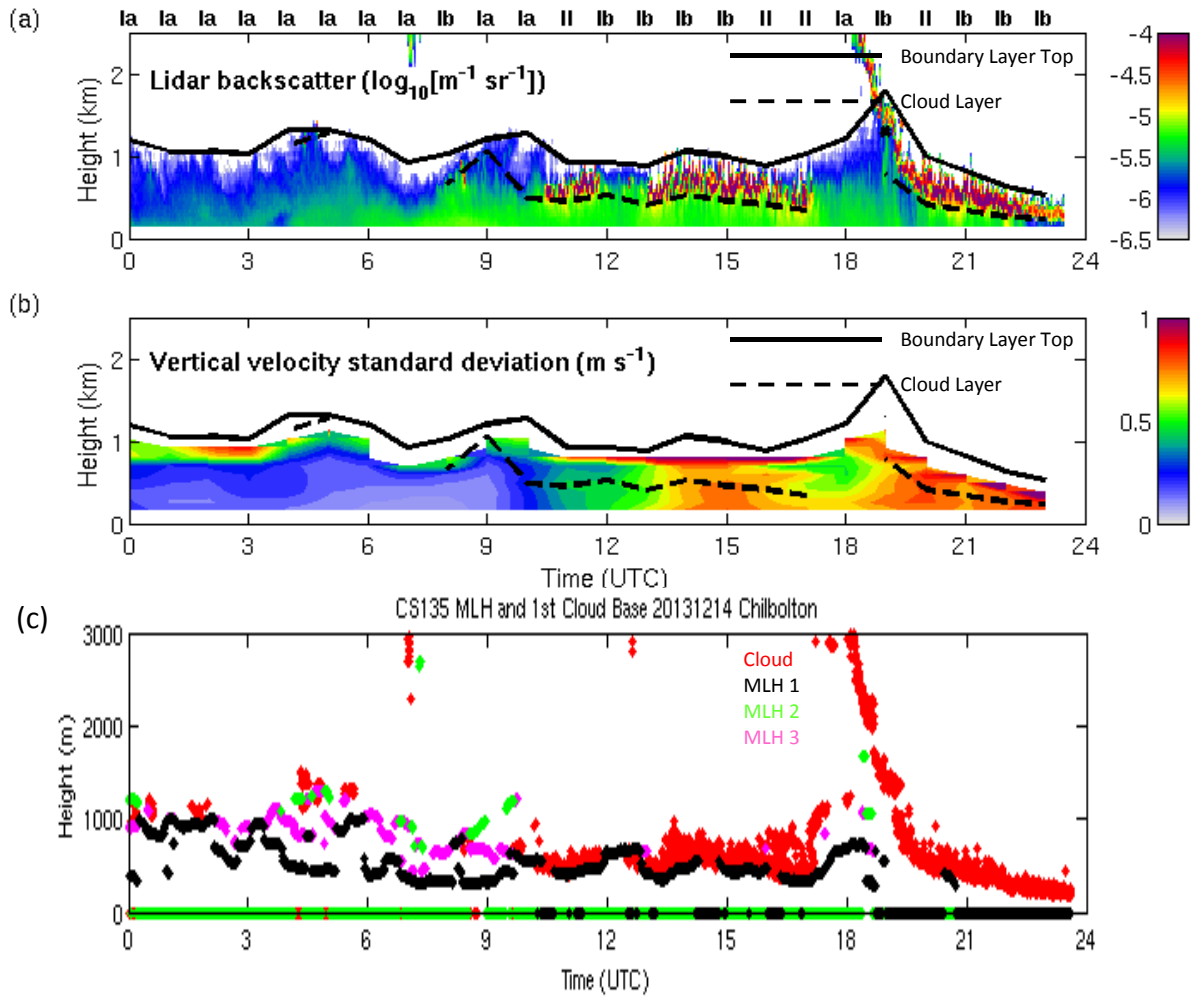

FIG. 5. Same as Fig. 2 except from 14 December 2013. Here at least one mixing layer was reported throughout most of the day, even when cloud was present. Judging from the backscatter profile in panel a) it appears that the cloud layer between 10:00 and 17:00 was atop the mixed layer, and the Harvey algorithm classified the boundary layer as a stratus-topped stable layer during most of this time. As with the previous example, in the presence of very low cloud (between 21:00 and 24:00) no mixing layer height was reported.

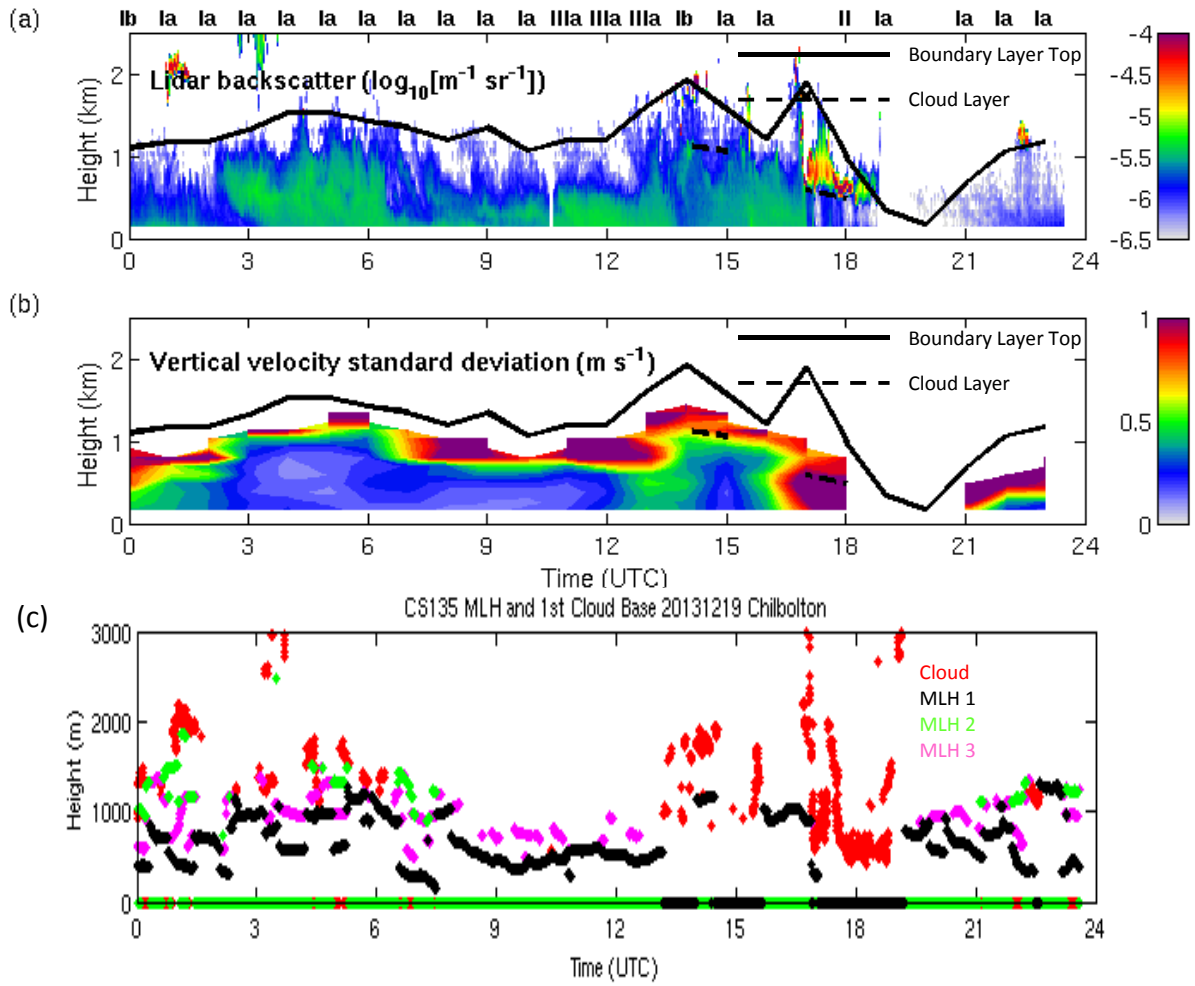

FIG. 6. Same as Fig. 2 except from 19 December 2013. At least one mixing layer height was reported throughout most of the day, tracking the aerosol layers visible in the Doppler backscatter signal. No MLH was reported between 17:00 and 19:00 when it was raining.

4. PRELIMINARY ANALYSIS

During the month of December, the CS135 reported MLH 52% of the time. The CS135 reported cloud base 64% of the time. Of the MLH reports, 53% were reported when a cloud base was detected and 47% when no cloud was detected. Histograms of the reported layers are shown in Fig. 7.

In Fig. 7, panels a) and b) show the automated mixing layer heights reported by the CS135 for all cases and for cloud free cases, respectively. Here the roughly lognormal distribution shows little change between the two sets aside from scaling, so cloud base did not appear shift the distribution of MLH measurements. Note that to create panel b), CS135 cloud base and MLH reports were compared every 10 seconds even though the MLH running average was 30 minutes, which is not an optimum approach when considering intermittent cloud situations.

Panels c) and d) show the top of the planetary boundary layer (PBL) derived from the Doppler lidar backscatter signal by the Harvey code for all cases and cloud free cases, respectively. In the Harvey code, boundary layer depth is found by locating the first “aerosol-free” range bin where 80% of lidar aerosol backscatter returns are zero. This is applied both in the presence and absence of clouds which means that if dense clouds are present, the boundary layer top will be assigned in the cloud. Since the lidar-based PBL retrieval looks for the clear air signal, rather than the steepest gradient, it is expected that the lidar PBL height would be higher than the CS135 MLH. On average, PBL was reported 446m above the MLH with a standard deviation of 431m. In cloud free conditions the lidar PBL was reported 348m above the CS135 MLH, with a standard deviation of 394m. The conclusion here is that while the PBL height reported is generally higher than the MLH, the two measurements do not track each other with a simple offset.

Panels f) and g) show the lowest cloud base reported by the CS135 and the cloud base derived from the Doppler lidar by the Harvey code, respectively. Both histograms suggest bimodal distributions with peaks at around 250m and 750m.

Panel h) shows the distribution of PBL types described in Table 2 derived from the Doppler lidar and sonic anemometer measurements using the Harvey code, while panel i) shows the distribution of types only when the CS135 MLH was reported. Here the distributions are similar, except that the peak of the distribution, type Ia (stable, no cloud), increases from approximately 1.5 times the next most frequent layer, Ib, when all outputs are considered to roughly 4 times Ib when only cases where MLH is reported are considered. This means that the likelihood that the CS135 MLH will be reported is increased in situations identified as stable without clouds. Since the aerosol concentration is likely to be higher (and thus the backscatter gradient steeper) in stable situations than under mixed conditions, it is not surprising that MLH would be more likely to be reported for stable boundary layers. However, only the cloud free stable situation is disproportionately scaled in panel i). This suggests that cloud may be influencing the CS135’s ability to detect MLH in one of three ways: 1) gain and thus sensitivity are automatically decreased when clouds are present to avoid detector saturation which could decrease sensitivity to aerosols; 2) the aerosol layer blends into the cloud layer making the aerosol gradient difficult to detect; 3) the cloud filtering step shown in Fig. 1 which is applied prior to the gradient detection algorithm is also filtering out aerosol gradients from the signal. Further investigation is required in order to understand this, and to improve the CS135 sensitivity when clouds are present. Note that during a three year analysis performed by Harvey et al. (2013), stable conditions without cloud were also the most common type retrieved by the Doppler lidar anemometer algorithm at Chilbolton Observatory, but types II through VI are represented proportionately more often than they were during the one month of winter data analysed in this paper.

5. CONCLUSIONS

In this paper a new automated mixing layer height algorithm for a ceilometer, the Campbell Scientific CS135, has been described. Preliminary results of a trial alongside a HALO Photonics Doppler lidar system during a winter month at the Chilbolton Observatory in Hampshire, UK have been presented. A boundary layer classification scheme developed by Harvey et al. (2013) has been applied to Doppler lidar and sonic anemometer data to assess whether the ceilometer was more likely to report mixing layer height during different types of boundary layer conditions. It was found that the probability of the ceilometer algorithm reporting MLH was enhanced when the PBL was classified as being stable and cloud free. The ceilometer MLH detection has been shown to function under a variety of aerosol loads and in cloudy conditions. Further work includes analysis of a multi-seasonal data set, an investigation of how the reported ceilometer mixing layer heights relate to vertical velocity variance derived from the Doppler lidar signal, and application of the CS135 MLH algorithm to other instruments for comparison.

ACKNOWLEDGEMENTS

The authors would like to acknowledge CFARR (the Chilbolton Facility for Atmospheric and Radio Research) for providing data, and Natalie Harvey at the University of Reading for publishing the PBL classification code.

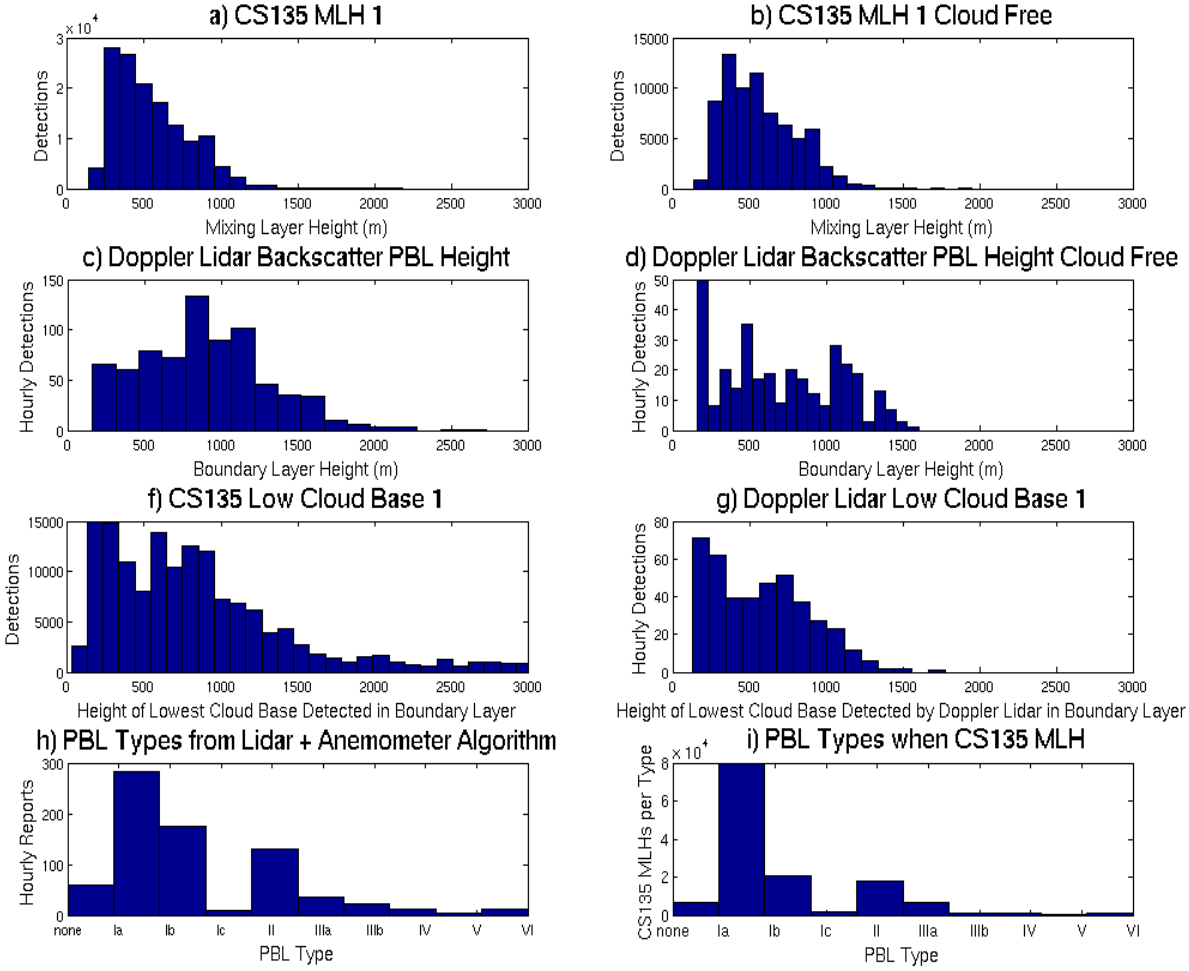

Fig. 7. PDFs of CS135 and Doppler Lidar Measurements from December 2013: a) Mixing layer heights reported by the CS135; b) Mixing layer heights reported by the CS135 in the absence of cloud; c) Boundary layer heights derived from Doppler lidar backscatter; d) Boundary layer heights derived from Doppler lidar backscatter in the absence of cloud; f) Lowest layer cloud base heights reported by the CS135 in the boundary layer; g) Cloud base derived from Doppler lidar backscatter; h) Boundary layer types reported from the Doppler lidar + sonic anemometer algorithm; i) Boundary layer types when the CS135 was reporting mixing layer height.

REFERENCES

Barlow, Janet F., T. M. Dunbar, E. G. Nemitz, C. R. Wood, M. W. Gallagher, F. Davies, E. O'Connor, and R. M. Harrison, 2011: Boundary layer dynamics over London, UK, as observed using Doppler lidar during REPARTEE-II. *Atmos. Chem.Phys.*, **11**(5), 2111-2125, doi: 10.5194/acp-11-2111-2011.

de Haij, M., W. Wauben, and H.K. Baltink, 2007: Continuous mixing layer height determination using the LD-40 ceilometer: a feasibility study. KNMI, De Bilt, Netherlands.

Haeffelin, M., and Coauthors, 2012: Evaluation of mixing-height retrievals from automatic profiling lidars and ceilometers in view of future integrated networks in Europe. *Bound.-Layer Meteor.* **143**(1), 49-75, 10.1007/s10546-011-9643-z.

Harvey, N. J., R. J. Hogan, and H. F. Dacre, 2013: A method to diagnose boundary-layer type using Doppler lidar. *Q. J. R. Meteorol. Soc.*, **139**(676), 1681-1693, doi 10.1002/qj.2068.

Harvey, N. J., accessed 2014: bl_type-0.1 MATLAB code. [Available online at http://www.met.reading.ac.uk/~py904867/research/BL_type_diagnosis.html.]

Holzworth, G. C., 1967: Mixing depths, wind speeds and air pollution potential for selected locations in the United States. *J. Appl. Meteor.*, **6**, 1039–1044, doi: 10.1175/1520-0450(1967)006<1039:MDWSAA>2.0.CO;2.

Lock, A. P., A. R. Brown, M. R. Bush, G. M. Martin, and R. N. B. Smith, 2000: A New Boundary Layer Mixing Scheme. Part I: Scheme Description and Single-Column Model Tests. *Mon. Wea. Rev.*, **128**, 3187–3199, doi: 10.1175/1520-0493(2000)128<3187:ANBLMS>2.0.CO;2.

Münkel, C. and J. Räsänen, 2004: New optical concept for commercial lidar ceilometers scanning the boundary layer, *Proc. SPIE*, **5571**, 364–374, doi 10.1117/12.565540.

O'Connor, E. J., A. J. Illingworth, I. M. Brooks, C. D. Westbrook, R. J. Hogan, F. Davies, and B. J. Brooks, 2010: A Method for Estimating the Turbulent Kinetic Energy Dissipation Rate from a Vertically Pointing Doppler Lidar, and Independent Evaluation from Balloon-Borne In Situ Measurements. *J. Atmos. Oceanic Technol.*, **27**, 1652–1664, doi: 10.1175/2010JTECHA1455.1.

Pearson, G., F. Davies, and C. Collier, 2009: An Analysis of the Performance of the UFAM Pulsed Doppler Lidar for Observing the Boundary Layer. *J. Atmos. Oceanic Technol.*, **26**, 240–250, doi 10.1175/2008JTECHA1128.1.

STFC, accessed 2014: Chilbolton HALO Photonics Doppler Lidar. [Available online at http://www.stfc.ac.uk/Chilbolton/24830.aspx.]

STFC, accessed 2014b: Chilbolton Metek USA-1 Sonic Anemometer. [Available online at http://www.stfc.ac.uk/Chilbolton/facilities/44003.aspx.]

Vande Hey, J., J. Coupland, M. Foo, J. Richards, and A. Sandford, 2011: Determination of overlap in lidar systems. *Appl. Opt.*, **50**, 5791-5797, doi 10.1364/AO.50.005791.

VandeHey, J., J. Coupland, J. Richards and A. Sandford, 2012: Design and implementation of a divided-lens lidar ceilometer prototype for manufacture. *Geoscience and Remote Sensing Symposium (IGARSS), 2012 IEEE International*, 5002-5005, doi 10.1109/IGARSS.2012.6352488.

Wiegner, M., S. Emeis, V. Freudenthaler, B. Heese, W. Junkermann, C. Münkel, K. Schäfer, M. Seefeldner and S. Vogt, 2006: Mixing layer height over Munich,
Germany: variability and comparisons of different methodologies. *J. Geophys. Res.*, **111**, D13, 16, doi:10.1029/2005JD006593.